Observations of anomalous x-ray emission at early stages of hot-spot formation in deuterium-tritium cryogenic implosions

R. C. Shah, S. X. Hu, I. V. Igumenshchev, J. Baltazar, D. Cao, C. J. Forrest, V. N. Goncharov, V. Gopalaswamy, D. Patel, F. Philippe, W. Theobald, and S. P. Regan

Phys. Rev. E **103**, 023201 — Published 1 February 2021

DOI: 10.1103/PhysRevE.103.023201

Observations of anomalous x-ray emission at early stages of hot-spot formation in DT cryogenic implosions

R. C. Shah,[1,*] S. X. Hu,[1] I. V. Igumenshchev,[1] J. Baltazar,[1] D. Cao,[1] C. J. Forrest,[1] V. N. Goncharov,[1] V. Gopalaswamy,[1] D. Patel,[1] F. Philippe,[2] W. Theobald,[1] and S. P. Regan[1]

[1] *Laboratory for Laser Energetics, University of Rochester, Rochester, NY 14623*

[2] *CEA, DAM, DIF, 91297 Arpajon Cedex, France*

(Dated: January 5, 2021)

In DT cryogenic implosions, hot-spot x-ray self-emission is observed to begin at a larger shell radius than is predicted by a 1-D radiation-hydrodynamic implosion model. Laser-imprint is shown to explain the observation for a low-adiabat implosion. For more-stable implosions the data are not described by the imprint model and suggest there are additional sources of decompression of the dense fuel.

On the 30-kJ OMEGA laser, experiments are conducted on spherical implosions so as to create conditions relevant to inertial confinement fusion. Plastic capsules ($\sim$1 mm in diameter) containing a cryogenic shell of solid deuterium–tritium (DT) fuel are directly imploded by $\sim$20 TW of laser power arriving via 60 beams. The dense shell acts as a piston to create a fusion-relevant pressure ($\sim$100 Gbar) and temperature ($\sim$3 to 5 keV) in DT plasma termed the hot spot. The OMEGA experiments are interpreted by hydrodynamic scaling to the $\sim$2-MJ National Ignition Facility (NIF) for which the implosion dimensions would be sufficiently large that hot-spot fusion reactions can cause runaway self-heating. Substantial progress has occurred [1] but the hot-spot conditions are not yet sufficient to trigger a self-sustained fusion reaction [2]. An impediment to progress is that well-supported hypotheses for the underperformance in these directly laser-driven implosions have not yet emerged.

A specific challenge of the direct-drive approach, in which laser light directly impinges on the ablator, is that the coherent speckle of the laser light acts as a source of perturbations at the ablation surface. While the rapid formation of a plasma conduction zone limits the seeding to the earliest times of the drive, the small perturbations are amplified by the Rayleigh–Taylor instability. If this growth is sufficient, the spherical shell of peripheral dense fuel is decompressed and creates a low-density tail extending into the hot spot; these factors reduce the dynamic pressure $p_{\mathrm{d}} = \rho_{\mathrm{sh}} v_{\mathrm{sh}}^2$ and stagnation hot-spot pressure $p_{\mathrm{hs}} \sim p_{\mathrm{d}}^{5/3}$, where ρ_{sh} and v_{sh} are shell density and velocity, respectively [3]. A limit on the shell density arises from entropy, which is determined in direct-drive implosions mainly by laser pulse shape and resulting shocks. It is characterized by adiabat α, defined as the ratio of the pressure to the Fermi-degenerate pressure at the shell density. Implosions having a higher adiabat and thicker fuel layers tend to be more robust at the expense of ideal 1-D performance. Experiments in fully plastic ablators without cryogenic layers have suggested imprint as modeled *is* a sufficient input to account for shell decompression [4–7]. As compared to warm implosions, the ignition targets are cryogenic and have only a very thin outer layer of plastic. Interior to this is a much thicker shell of DT ice, which functions as both ablator and dense fuel. In the cryogenic case, ablation in the solid-density DT mitigates the growth of the imprint induced perturbations due to increased ablative stabilization [8]. Other factors, such as debris (for which growth is highly non-linear) [9, 10], shock mistiming [11], and details of the DT shock-release physics (studied to date in plastic [12, 13]) may become important to the fuel decompression. However, testing such modeling in the cryogenic case is technically challenging as compared to the warm implosions given negligible opacity of hydrogen and an absence of a material interface to define the hot spot. This Letter describes the first such study made in DT targets.

In this work we diagnose hot-spot formation in integrated DT cryogenic implosions based on a detailed study of nascent x-ray self-emission from the hot-spot. The diagnostic signature arose from the observation that time-resolved images of soft x-ray self-emission showed an onset of the hot-spot emission at less convergence as compared to 1-D radiation-hydrodyanamic modeling. As noted by Hu *et al.* [7], such earlier onset of emission results from a relaxed, or thickened, density profile as may be caused by imprinting. By detailed comparison with 3-D radiation hydrodynamic modeling which includes a diffraction based model of the laser imprint, our time-gated work provides the first indication of laser-imprint damage of hot-spot assembly in a low-adiabat DT cryogenic implosion. However, we also find a persistence of the emission turn-on discrepancy in more-stable implosions for which it is not predicted by the model. The discrepancy is shown to reduce as the implosion stability is increased. These spatially resolved and time-integrated measurements suggest a modeling gap specific to the fuel assembly and its profile relaxation as the implosion enters deceleration.

We draw on six DT cryogenic implosion experiments (see Table I) for which the emission turn-on was analyzed from the framed image data and compared in detail to

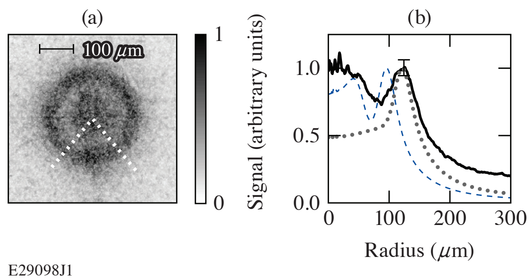

FIG. 1. (a) Observed soft x-ray self-emission at the onset of hot-spot core emission a cryogenic implosions experiment. The lower sector indicated by dotted white lines can include emission related to stalk mounting and is excluded from analysis. (b) Angle-averaged radial profile from the experimental image is shown by the solid black curve. The result from 1-D modeling at matched position of the ablation front is shown with the dotted black curve. The dashed cyan curve shows the 1-D result obtained ~70 ps later at which time the center emission reaches the prominence observed in the data.

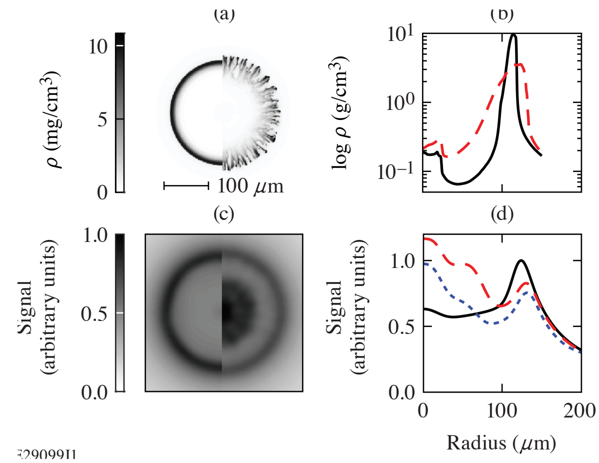

FIG. 2. 3-D *ASTER* results. (a) Density for uniform (left) and imprint simulations (right). (b) Angle average of mass density (uniform, solid black curve; imprint, red dashed curve). (c) Self-emission images and (d) angle-averaged emission profiles (same formatting as in (c). The dotted blue curve excludes carbon emission interior to radial values less than 200 μm.

models. The targets nominally had outer diameters of 870 μm with 8-μm CD shell, DT layer thicknesses of 50 or 65 μm, and DT ratio of 50:50 or 70:30. The total on-target laser energy varied between 17.5 to 21 kJ. Other parameters of the 60-beam experiments at the OMEGA laser such as phase-plates and beam smoothing were unchanged from recent publications [1, 14]. The design choices of the targets and specific details of the single-picket pulse shapes provide for variations of stability via both α and in-flight aspect ratio (IFAR), which is the ratio of the shell radius to shell thickness at two-thirds initial radius. A convenient single metric is an empirical instability parameter given by $S = \mathrm{IFAR}/\alpha^{1.1}$ [3] for which higher values indicate a less stable implosion .

An example of the aforementioned motivating observation is shown in Fig. 1. Figure 1(a) shows a 40 ps gated pinhole image of soft x-ray self-emission (~800 eV) taken from shot 94008. The image is corrected for 6× magnification, film response, background and measurement artifacts. As the thin shell of CD has been ablated away by this phase of the implosion, the image shows a single

TABLE I. Summary of 1-D *LILAC* calculated α, IFAR, instability parameter S=IFAR/$\alpha^{1.1}$, and yield Y for the DT cryogenic implosions for which the hot-spot emission onset has been analyzed. Measured yield is noted in parentheses.

S	Shot	α	IFAR	Y ($\times 10^{14}$)
2.9	79626	5.8	19.9	0.3 (0.18)
3.4	79624	4.7	18.6	0.45 (0.21)
6.0	91547	3.3	22.3	1.7 (0.39)
6.9	94017	2.9	22.3	0.88 (0.12)
7.9	94008	2.8	24.5	1.7 (0.29)
21.8	94013	1.7	39	2.8 (0.14)

peripheral emission limb associated with laser absorption and ablation in high-density DT fuel [15]. Interior to the ablation-front emission is an annulus of reduced emission at the position of dense fuel, and, finally, a center brightening due to the heating of lower-density hydrogen which forms the hot spot. The sector demarcated by the dashed white lines encompasses the position of target mounting and is excluded from analysis. After identifying the best-fit circle for the emission limb, the image is averaged around this center to produce the angle-averaged profile shown as the solid black line in Fig. 1(b). The result of synthetic image analysis based on 1-D radiation-hydrodynamic code *LILAC* [16] and which accounts for spectral response, 40 ps time-gating, and 20-μm spatial resolution of the experiment [17] is shown by the dotted black line. The calculated image is chosen to match the convergence of the experimental image and both images are normalized to the limb peak. There is a prominent discrepancy in the level of hot-spot emission at r <100 μm. The result from the 1-D simulation at a time 70 ps later is shown by the dashed cyan line. Additional convergence is required in the simulation to reach a comparable hot-spot emission. Even then, the result from the simulation shows a hot-spot emission profile with an edge peaking that contrasts the center peaked result from experiment. The onset of the hot-spot emission serves as our diagnostic signature related to hot-spot formation and is discussed extensively in the remainder of the Letter.

We next consider modeling in which the dense fuel is strongly perturbed by laser imprint to illustrate how enhanced hot-spot emission results from a relaxation of the dense fuel profile. For this modeling we have used the

3-D radiation-hydrodynamic code $ASTER$ [18], an Eulerian code that uses the speckle calculated from diffraction theory to modulate the incident beams [19]. It has been run so as to sufficiently resolve Legendre modes up to $\ell \simeq 200$, as was previously used to study imprint [20]. The model further accounts for all aspects of beam smoothing deployed in the experiments: distributed phase plates [21, 22], polarization smoothing [23], and smoothing by spectral dispersion [24, 25]. The results from $ASTER$ are in qualitative agreement with additional 2-D simulations using the $DRACO$ code [26]. In Fig. 2 we examine results from application of this model to low stability $S = 21.8$ implosion ($\alpha = 1.7$) for which there is a neutron yield reduction of $\sim$90% when comparing the 3-D calculations with and without imprinting. Figure 2(a) contrasts the density profile determined from $ASTER$ for the uniform (left) and imprint (right) models at a time at which the hot-spot emission predicted with imprint becomes prominent. Angle averages of these profiles (uniform, solid black and imprint, red dashed curves) are shown on a logarithmic scale in Fig. 2(b). The returning shock has not yet collided with the inbound high-density fuel and is clearly visible at $r \sim 25$ μm in both models. The density profile for the imprint case exhibits decompression, which is accompanied by a density tail deep into the core. The chord-integrated self-emission images are shown in Fig. 2(c) and corresponding angle averages in Fig. 2(d). The additional curve in Fig. 2(d) (dotted blue line) is the result of a second imprint simulation excluding emission from mixed CD within a radius less than 200 μm (the exclusion of the CD emission from the hot spot did not further change the modeled neutron yield). The advance in emission onset relative to ablation radius for the imprint model is the result of several contributions. Foremost, the density tail [Figs. 3(a) and 3(b)] leads to earlier compressive work and pressure buildup. Other contributions are also attributed to the hydrodynamic instability: a broadened and therefore weaker emission limb; carbon enhancement of the emission; and an outward shift of the ablation front.

To quantify the early onset of the hot-spot emission we have tracked its increase as a function of ablation front position. The detailed comparison of this evolution with post-shot $ASTER$ simulations is shown for two companion shots, with instability parameter $S = 21.8$ [Fig. 3(a)] and $S = 7.9$ [Fig. 3(b)]. These shots occurred with nominally identical targets and both implosions were driven with single-picket pulses with nearly matched drive energy (25 kJ) and peak drive power (20 TW). For the $S = 21.8$ implosion the picket power was $\sim$2 TW giving design $\alpha = 1.7$. In contrast, the $S = 7.9$ case had approximately twice the power in the picket and shorter delay between picket and main resulting in $\alpha = 2.8$. The relative core emission is calculated from each framed image as $\frac{2}{(R_{\mathrm{pk}}/2)^2}\int_0^{R_{\mathrm{pk}}/2} rI(r)\mathrm{d}r$, where $I(r)$ is the angle averaged

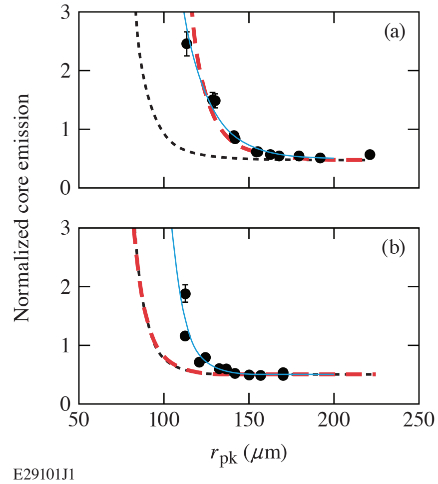

FIG. 3. Central emission versus inferred ablation front radius for (a) $S = 21.8$, $\alpha = 1.7$, and (b) $S = 7.9$, $\alpha = 2.8$ implosions. Data are indicated by solid circles with cyan line showing fit. Results from uniform $ASTER$ are indicated by dotted black line for all three cases. High-resolution $ASTER$ with laser imprinting is shown by dashed red line.

signal normalized to the peak at the emission limb and R_{pk} is the peak position of the limb. In the plots of Fig. 3, the solid black circles and cyan line correspond to the experimental measurements and fit; the dotted black line is the uniform $ASTER$ calculation; and the red dashed line is the $ASTER$ model including imprint. The data and simulation are fit using a delayed exponential with constant offset. After correcting for slight variations of the offset the emission onset is determined at the position of unity normalized emission. We find for the lower stability $S = 21.8$ case [Fig. 3(a)] this turn-on occurs at R_{pk}=137$\pm$2 μm (error is assumed dominated by the radial determination). The measured emission onset occurs at a radius that is 38 μm larger than what is determined by the identical analysis of the uniform $ASTER$ calculation. For this lower stability case, the imprint calculation (dashed red line) shows an emission onset at 134 μm, in close agreement with the measurement. Figure 3(b) shows the corresponding evolution of the core emission for the $S = 7.9$ higher stability companion. The onset of hot-spot emission from the experiment is at a smaller radius of 118$\pm$2 μm but remains discrepant with the uniform calculation by 23 μm. As compared to the 90% reduction in calculated yield due to imprint for $S = 21.8$, the yield reduction is 22% for the $S = 7.9$ calculation. In the higher-stability case there is no significant modification of the calculated turn-on radius and the imprint model does not provide an explanation for the observation.

To examine this discrepancy over more shots and greater range of the instability parameter S, the shift

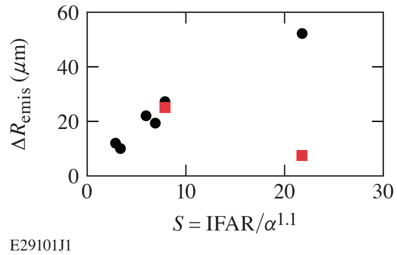

FIG. 4. Survey of six implosions of Table I showing difference in measured onset of hot-spot emission as compared to models (ΔR_{emis}) versus instability parameter (S). The comparison relative to 1-D *LILAC* is indicated by black circles and relative to 3-D *ASTER* with imprint by the red squares (two available cases only).

in emission turn-on (ΔR_{emis}) was determined for the six implosions of Table I as compared to their post-shot 1-D *LILAC* simulations (see Fig. 4, black circles). The comparison of the emission turn-on relative to the 3-D *ASTER* simulations with imprint, for the two available cases, is shown with the red squares. Imprint provides an explanation, due to profile relaxation and shell breakup, for the right-most point at $S = 21.8$. However, the imprint model cannot explain any part of the measurement at $S = 7.9$ (and by extension smaller values of S). At present we cannot exclude the possibility of shock related processes in causing a relaxed fuel profile; however, the clear dependence on a stability parameter more strongly supports unmodeled additional perturbations which seed Rayleigh-Taylor growth such as debris (which may cause rapid development of highly nonlinear phases of the instability [10]) or ice roughness. To help differentiate these hypothesis, future studies are being planned which will use careful matching of shock driven adiabat for implosions with contrasting layer thicknesses (thereby varying S). Furthermore, target characterizations using a new capability to microscopically examine plastic debris and damage following cryogenic fill [27] will be compared against the experimental signatures.

In summary, we have presented time and space resolved characterization of the onset of x-ray emission from the hot-spot plasma in direct-drive experiments of cryogenic spherical implosions. The measurements are taken in-flight at convergence ratio of $\sim$3, thereby emphasizing conditions at the start of deceleration. With respect to understanding current limitations on hot-spot performance, the x-ray emission onset provides first evidence of good agreement with a 3-D radiation-hydrodynamic model of laser imprint in a low-adiabat, integrated DT cryogenic implosion. However, as the emission discrepancies are not explained for more stable implosions, these results are also suggestive of an understanding gap specific to modeling of early fuel assembly and profile relaxation.

This work is supported by the Department of Energy National Nuclear Security Administration under Award No. DE-NA0003856, the University of Rochester, and the New York State Energy Research and Development Authority.

* rahulshah@lle.rochester.edu

[1] V. Gopalaswamy, R. Betti, J. P. Knauer, N. Luciani, D. Patel, K. M. Woo, A. Bose, I. V. Igumenshchev, E. M. Campbell, K. S. Anderson, K. A. Bauer, M. J. Bonino, D. Cao, A. R. Christopherson, G. W. Collins, T. J. B. Collins, J. R. Davies, J. A. Delettrez, D. H. Edgell, R. Epstein, C. J. Forrest, D. H. Froula, V. Y. Glebov, V. N. Goncharov, D. R. Harding, S. X. Hu, D. W. Jacobs-Perkins, R. T. Janezic, J. H. Kelly, O. M. Mannion, A. Maximov, F. J. Marshall, D. T. Michel, S. Miller, S. F. B. Morse, J. Palastro, J. Peebles, P. B. Radha, S. P. Regan, S. Sampat, T. C. Sangster, A. B. Sefkow, W. Seka, R. C. Shah, W. T. Shmyada, A. Shvydky, C. Stoeckl, A. A. Solodov, W. Theobald, J. D. Zuegel, M. G. Johnson, R. D. Petrasso, C. K. Li, and J. A. Frenje, Tripled yield in direct-drive laser fusion through statistical modelling, Nature **565**, 581 (2019).

[2] R. Betti, A. R. Christopherson, B. K. Spears, R. Nora, A. Bose, J. Howard, K. M. Woo, M. J. Edwards, and J. Sanz, Alpha heating and burning plasmas in inertial confinement fusion, Phys. Rev. Lett. **114**, 255003 (2015).

[3] V. N. Goncharov, T. C. Sangster, R. Betti, T. R. Boehly, M. J. Bonino, T. J. B. Collins, R. S. Craxton, J. A. Delettrez, D. H. Edgell, R. Epstein, R. K. Follett, C. J. Forrest, D. H. Froula, V. Yu. Glebov, D. R. Harding, R. J. Henchen, S. X. Hu, I. V. Igumenshchev, R. Janezic, J. H. Kelly, T. J. Kessler, T. Z. Kosc, S. J. Loucks, J. A. Marozas, F. J. Marshall, A. V. Maximov, R. L. McCrory, P. W. McKenty, D. D. Meyerhofer, D. T. Michel, J. F. Myatt, R. Nora, P. B. Radha, S. P. Regan, W. Seka, W. T. Shmayda, R. W. Short, A. Shvydky, S. Skupsky, C. Stoeckl, B. Yaakobi, J. A. Frenje, M. Gatu-Johnson, R. D. Petrasso, and D. T. Casey, Improving the hot-spot pressure and demonstrating ignition hydrodynamic equivalence in cryogenic deuteriumtritium implosions on omega, Physics of Plasmas **21**, 056315 (2014), https://doi.org/10.1063/1.4876618.

[4] V. A. Smalyuk, S. X. Hu, J. D. Hager, J. A. Delettrez, D. D. Meyerhofer, T. C. Sangster, and D. Shvarts, Rayleigh-taylor growth measurements in the acceleration phase of spherical implosions on omega, Phys. Rev. Lett. **103**, 105001 (2009).

[5] S. X. Hu, G. Fiksel, V. N. Goncharov, S. Skupsky, D. D. Meyerhofer, and V. A. Smalyuk, Mitigating laser imprint in direct-drive inertial confinement fusion implosions with high-z dopants, Phys. Rev. Lett. **108**, 195003 (2012).

[6] D. T. Michel, S. X. Hu, A. K. Davis, V. Y. Glebov, V. N. Goncharov, I. V. Igumenshchev, P. B. Radha, C. Stoeckl, and D. H. Froula, Measurement of the shell decompression in direct-drive inertial-confinement-fusion implosions, Phys. Rev. E **95**, 051202 (2017).

[7] S. X. Hu, D. T. Michel, A. K. Davis, R. Betti, P. B. Radha, E. M. Campbell, D. H. Froula, and C. Stoeckl, Understanding the effects of laser imprint on plastic-target implosions on omega, Physics of Plasmas **23**, 102701 (2016), https://doi.org/10.1063/1.4962993.

[8] S. Atzeni and J. Meyer-ter-vehn, *The Physics of Inertial Confinement Fusion* (Oxford University Press, Oxford, 2004).

[9] T. C. Sangster, V. N. Goncharov, R. Betti, P. B. Radha, T. R. Boehly, D. T. Casey, T. J. B. Collins, R. S. Craxton, J. A. Delettrez, D. H. Edgell, R. Epstein, C. J. Forrest, J. A. Frenje, D. H. Froula, M. Gatu-Johnson, Y. Y. Glebov, D. R. Harding, M. Hohenberger, S. X. Hu, I. V. Igumenshchev, R. Janezic, J. H. Kelly, T. J. Kessler, C. Kingsley, T. Z. Kosc, J. P. Knauer, S. J. Loucks, J. A. Marozas, F. J. Marshall, A. V. Maximov, R. L. McCrory, P. W. McKenty, D. D. Meyerhofer, D. T. Michel, J. F. Myatt, R. D. Petrasso, S. P. Regan, W. Seka, W. T. Shmayda, R. W. Short, A. Shvydky, S. Skupsky, J. M. Soures, C. Stoeckl, W. Theobald, V. Versteeg, B. Yaakobi, and J. D. Zuegel, Improving cryogenic deuteriumtritium implosion performance on omega, Physics of Plasmas **20**, 056317 (2013), https://doi.org/10.1063/1.4805088.

[10] I. V. Igumenshchev, V. N. Goncharov, W. T. Shmayda, D. R. Harding, T. C. Sangster, and D. D. Meyerhofer, Effects of local defect growth in direct-drive cryogenic implosions on omega, Physics of Plasmas **20**, 082703 (2013), https://doi.org/10.1063/1.4818280.

[11] V. N. Goncharov, T. C. Sangster, T. R. Boehly, S. X. Hu, I. V. Igumenshchev, F. J. Marshall, R. L. McCrory, D. D. Meyerhofer, P. B. Radha, W. Seka, S. Skupsky, C. Stoeckl, D. T. Casey, J. A. Frenje, and R. D. Petrasso, Demonstration of the highest deuterium-tritium areal density using multiple-picket cryogenic designs on omega, Phys. Rev. Lett. **104**, 165001 (2010).

[12] D. Haberberger, A. Shvydky, V. N. Goncharov, D. Cao, J. Carroll-Nellenback, S. X. Hu, S. T. Ivancic, V. V. Karaseiv, J. P. Knauer, A. V. Maximov, and D. H. Froula, Plasma density measurements of the inner shell release, Phys. Rev. Lett. **123**, 235001 (2019).

[13] S. Zhang and S. X. Hu, Species separation and hydrogen streaming upon shock release from polystyrene under inertial confinement fusion conditions, Phys. Rev. Lett. **125**, 105001 (2020).

[14] S. P. Regan, V. N. Goncharov, I. V. Igumenshchev, T. C. Sangster, R. Betti, A. Bose, T. R. Boehly, M. J. Bonino, E. M. Campbell, D. Cao, T. J. B. Collins, R. S. Craxton, A. K. Davis, J. A. Delettrez, D. H. Edgell, R. Epstein, C. J. Forrest, J. A. Frenje, D. H. Froula, M. Gatu Johnson, V. Y. Glebov, D. R. Harding, M. Hohenberger, S. X. Hu, D. Jacobs-Perkins, R. Janezic, M. Karasik, R. L. Keck, J. H. Kelly, T. J. Kessler, J. P. Knauer, T. Z. Kosc, S. J. Loucks, J. A. Marozas, F. J. Marshall, R. L. McCrory, P. W. McKenty, D. D. Meyerhofer, D. T. Michel, J. F. Myatt, S. P. Obenschain, R. D. Petrasso, P. B. Radha, B. Rice, M. J. Rosenberg, A. J. Schmitt, M. J. Schmitt, W. Seka, W. T. Shmayda, M. J. Shoup, A. Shvydky, S. Skupsky, A. A. Solodov, C. Stoeckl, W. Theobald, J. Ulreich, M. D. Wittman, K. M. Woo, B. Yaakobi, and J. D. Zuegel, Demonstration of fuel hot-spot pressure in excess of 50 gbar for direct-drive, layered deuterium-tritium implosions on omega, Phys. Rev. Lett. **117**, 025001 (2016).

[15] D. T. Michel, A. K. Davis, V. N. Goncharov, T. C. Sangster, S. X. Hu, I. V. Igumenshchev, D. D. Meyerhofer, W. Seka, and D. H. Froula, Measurements of the conduction-zone length and mass ablation rate in cryogenic direct-drive implosions on omega, Phys. Rev. Lett. **114**, 155002 (2015).

[16] J. Delettrez, R. Epstein, M. C. Richardson, P. A. Jaanimagi, and B. L. Henke, Effect of laser illumination nonuniformity on the analysis of time-resolved x-ray measurements in uv spherical transport experiments, Phys. Rev. A **36**, 3926 (1987).

[17] A. K. Davis, Ph.D. thesis, University of Rochester (2017).

[18] I. V. Igumenshchev, V. N. Goncharov, F. J. Marshall, J. P. Knauer, E. M. Campbell, C. J. Forrest, D. H. Froula, V. Y. Glebov, R. L. McCrory, S. P. Regan, T. C. Sangster, S. Skupsky, and C. Stoeckl, Three-dimensional modeling of direct-drive cryogenic implosions on omega, Physics of Plasmas **23**, 052702 (2016), https://doi.org/10.1063/1.4948418.

[19] R. Epstein, Reduction of time-averaged irradiation speckle nonuniformity in laser-driven plasmas due to target ablation, Journal of Applied Physics **82**, 2123 (1997), https://doi.org/10.1063/1.366021.

[20] I. V. Igumenshchev, A. L. Velikovich, V. N. Goncharov, R. Betti, E. M. Campbell, J. P. Knauer, S. P. Regan, A. J. Schmitt, R. C. Shah, and A. Shvydky, Rarefaction flows and mitigation of imprint in direct-drive implosions, Phys. Rev. Lett. **123**, 065001 (2019).

[21] Y. Kato, K. Mima, N. Miyanaga, S. Arinaga, Y. Kitagawa, M. Nakatsuka, and C. Yamanaka, Random phasing of high-power lasers for uniform target acceleration and plasma-instability suppression, Phys. Rev. Lett. **53**, 1057 (1984).

[22] T. J. Kessler, Y. Lin, J. J. Armstrong, and B. Velazquez, Phase conversion of lasers with low-loss distributed phase plates, in *Laser Coherence Control: Technology and Applications*, Vol. 1870, edited by H. T. Powell and T. J. Kessler, International Society for Optics and Photonics (SPIE, 1993) pp. 95 – 104.

[23] T. R. Boehly, V. A. Smalyuk, D. D. Meyerhofer, J. P. Knauer, D. K. Bradley, R. S. Craxton, M. J. Guardalben, S. Skupsky, and T. J. Kessler, Reduction of laser imprinting using polarization smoothing on a solid-state fusion laser, Journal of Applied Physics **85**, 3444 (1999), https://doi.org/10.1063/1.369702.

[24] S. Skupsky and R. S. Craxton, Irradiation uniformity for high-compression laser-fusion experiments, Physics of Plasmas **6**, 2157 (1999), https://doi.org/10.1063/1.873501.

[25] S. P. Regan, J. A. Marozas, J. H. Kelly, T. R. Boehly, W. R. Donaldson, P. A. Jaanimagi, R. L. Keck, T. J. Kessler, D. D. Meyerhofer, W. Seka, S. Skupsky, and V. A. Smalyuk, Experimental investigation of smoothing by spectral dispersion, J. Opt. Soc. Am. B **17**, 1483 (2000).

[26] S. X. Hu, V. N. Goncharov, P. B. Radha, J. A. Marozas, S. Skupsky, T. R. Boehly, T. C. Sangster, D. D. Meyerhofer, and R. L. McCrory, Two-dimensional simulations of the neutron yield in cryogenic deuterium-tritium implosions on omega, Physics of Plasmas **17**, 102706 (2010), https://doi.org/10.1063/1.3491467.

[27] R. Janezic, D. Bredesen, and M. Wittman (2020), internal Correspondence.